

Ground cracks development and characteristics of strata movement under fast excavation: a case study at Bulianta coal mine, China

Yuankun Xu¹ · Kan Wu¹ · Liang Li¹ · Dawei Zhou¹ · Zhenqi Hu²

Received: 29 November 2016 / Accepted: 1 April 2017 / Published online: 20 April 2017
© Springer-Verlag Berlin Heidelberg 2017

Abstract Field examples of fast exploitation from underground coal seams in Bulianta mines, China, show that unexpected developmental rules of settlement and cracks can occur. In situ observation and a physical model consisting of sand, plaster, mica, and calcium carbonate were jointly employed to study the movement of strata, as well as the developmental characteristics of surface cracks. The physical model was observed with a high-precision industrial photogrammetric system. The results indicate that ground cracks are caused by strata deformation, but the formation of ground cracks can, in turn, promote the deformation of strata. Moreover, by contrast with coal mining at a speed of about 2 m/day, we found that the ground does not achieve full subsidence until the advancing distance exceeds 2.2 times the mining depth under rapid excavation (approximately 12 m/day), which would cause large errors for surface settlement

prediction. OCF (opening and closing fractures) above gobs are self-closing, but the duration of the closing phase is 3.6 times that of the opening phase, different from the symmetric distribution caused by mining with slower speed. The whole developmental cycle is inversely proportional to mining speed, and fast excavation can shorten development time of OCF. However, the horizontal tension deformation is the most stable factor for predicting ground cracks regardless of excavation speed. The research results can provide theoretical basis for dynamic prediction of ground subsidence and cracks development caused by underground coal mining.

Keywords Surface crack · Physical model · Longwall mining · Subsidence · Coal exploitation

✉ Kan Wu
wukan6899@163.com

Yuankun Xu
xuyuankun5200@163.com

Liang Li
cumtliang@cumt.edu.cn

Dawei Zhou
531137384@qq.com

Zhenqi Hu
huzhenqi53@163.com

¹ School of Environmental Science and Spatial Informatics, China University of Mining and Technology, Xuzhou 221116, People's Republic of China

² Institute of Land Reclamation and Ecological Restoration, China University of Mining and Technology (Beijing), Beijing 100083, People's Republic of China

Introduction

The Shendong coalfield is one of the eight largest coalfields of the world, and its annual output is approximately 200 million tons. The coalfield is located in a typical eolian sand area of western China, where the ecological environment is fragile. Underground coal mining would cause plenty of ground fissures, thereby exacerbating land damage and degeneration. Moreover, the excavation speed of coal seams in Shendong coalfield exceeds 12 m/day, while that in coal mines of eastern China is generally less than 5 m/day. Because of the difference in excavation speed, the ground cracks and strata movement in Shendong coalfield have unique development rules.

There have been some studies investigating ground cracks and strata deformation induced by underground coal mining. Ni and Wang (2014) conducted a field measurement of ground cracks in Baodian mines, China (the mining speed is 2 m/day), and found that mining-induced surface cracks undergo a

symmetrical “opening-closure” development cycle, namely, the opening stage takes almost the same time as the closure stage. Fan et al. (2015) analyzed the distribution characteristics of surface fissures in the Yushenfu mines at Shaanxi province of China through remote sensing interpretation and field measurement. Wu et al. (1997) provided a theoretical formula for computing the occurrence position and maximum depth of fissures, and the test results indicated that it matched well with the field observation at Xinzizhuang mines of eastern China. In terms of strata movement and ground subsidence, He et al. (1991) analyzed a large amount of field data of mining-induced ground subsidence in China (where the mining speed is less than 2 m/day), and pointed out that the ground will reach full subsidence when the working face advances to 1.2–1.4 times the mining depth; this conclusion has been further verified in several similar studies (Cui et al. 1999; Deng et al. 2014).

The above-mentioned studies focused on either the surface fissures or strata movement yet paid little attention to the relationship between them. The influence of excavation speed was not taken into account as well. In this study, we used a physical model and continuous observation to explore the relationship between strata movement and ground cracks development. Furthermore, we analyzed the influence of mining speed using in situ observation and found some unique features of ground cracks and strata deformation caused by rapid excavation.

Prototype for the physical model

The Bulianta mine of the Shendong coalfield was selected to be the prototype for the physical model. Situated in Erdos, China, adjacent to the Maowusuo desert (Fig. 1), Bulianta is a semiarid area with an annual precipitation of 413.5 mm and



Fig. 1 A is the location of research area

an evaporation capacity of 2111.2 mm. Mechanized longwall mining is adopted by this colliery.

The average length of the working face in the Bulianta colliery is 3000 m and the width is 300 m. The coal seam has a thickness of 5 m, a burial depth of 190–220 m, and a dip angle of 1–3°. The immediate roof above the coal seam is 5 m thick, horizontally bedded, and contains a thin layer of fine sandstone. The main roof is predominantly composed of siltstone that contains thick sandy mudstone layers. The average roof thickness is 181.6 m. The near-surface unconsolidated layer is principally composed of 17 m of eolian sandy soil. The detailed structure and mechanical parameters of the rock strata is shown in Table 1. As the geometric size of the physical model only takes up 1/200 of the prototype, we expanded the coal seam thickness of the physical model to 7 m (translated to in situ situation) in order to observe the strata movement and ground cracks more clearly. We did not make any changes to the thickness of other strata in the physical model.

Methodology

Physical modeling with similar material

Physical modeling is one of the most effective methods to study ground destruction induced by underground coal exploitation (Whittaker and Reddish 1989) and is often used to simulate strata damage and other dynamic process caused by coal mining (Dai et al. 2010; Liu et al. 2011; Whittaker et al. 1985). In this experiment, a gravity-load mixed model formed of sand, plaster, and calcium carbonate was adopted (Wu et al. 2015).

Similarity theory

There are large differences between laboratory physical models and field coal mines in size. To reflect the important physical properties of the prototype (e.g. mechanical and kinetic characters), the similarity coefficients between the prototype and the physical model must satisfy the principles of similarity theory (Ghabraie et al. 2015; Liu et al. 2011). The strength similarity coefficient c_σ , geometry similarity coefficient c_L , and density similarity coefficient c_ρ can be computed as

$$c_\sigma = \frac{\sigma_p}{\sigma_m}; \quad c_L = \frac{L_p}{L_m}; \quad c_\rho = \frac{\rho_p}{\rho_m} \quad (1)$$

Where the subscripts p and m denote the prototype and the physical model, respectively; σ denotes strength; L denotes size; and ρ denotes density.

Table 1 Strata structure and composition of physical model

No.	Rock type	Prototype Thickness (m)	Compressive strength (Mpa)		Density (kg/m ³)		Similar material composition (%)				Total weight (kg)
			σ_p	σ_m	ρ_p	ρ_m	Sand	Mica powder	plaster	Calcium carbonate	
1	Weathered sandstone	17	11.6	52	1580	1500	80	18	1.4	0.6	120.5
2	glutenite	14.35	36.6	101	2430	1500	71	23	1.8	4.2	101.7
3	Medium grained sandstone	33.07	45.3	150	2390	1500	70	22	2.4	5.6	232.6
4	Mudstone & Silty mudstone	1.53	22.3	74	2280	1500	80	17	2.2	0.8	10.8
5	Medium grained sandstone	10.19	45.3	150	2390	1500	70	22	2.4	5.6	72.3
6	glutenite	2.42	36.6	101	2430	1500	71	23	1.8	4.2	17.2
7	Fine sandstone	4.45	44.6	128	2500	1500	79	16	2.5	2.5	31.5
8	glutenite	16.24	36.6	101	2430	1500	71	23	1.8	4.2	115.1
9	Fine sandstone	7.27	44.6	128	2500	1500	79	16	2.5	2.5	51.6
10	Sandy mudstone	6.58	22.8	74	2240	1500	80	17	2.1	0.9	46.7
11	Mudstone & Silty mudstone	3.96	22.3	74	2280	1500	80	17	2.1	0.9	28.1
12	Silty mudstone	13.89	40.6	128	2460	1500	79	16	2.5	2.5	98.5
13	Silty mudstone	33.2	40.6	128	2460	1500	79	16	2.5	2.5	235.3
14	Coarse grained sandstone	7.62	36.6	101	2430	1500	71	23	1.8	4.2	54.0
15	Medium grained sandstone	3.74	45.3	150	2390	1500	70	22	2.4	5.6	26.5
16	Silty mudstone	3.4	40.6	128	2460	1500	79	16	2.5	2.5	24.1
17	Fine sandstone	3.66	44.6	128	2500	1500	79	16	2.5	2.5	26.0
18	Silty mudstone	6.16	40.6	128	2460	1500	79	16	2.5	2.5	43.6
19	Fine sandstone	1.59	44.6	128	2500	1500	79	16	2.5	2.5	11.3
20	Coal seam	7	10.5	52	1450	1500	80	18	1.4	0.6	49.7
21	Silty mudstone	5	40.6	128	2460	1500	79	16	2.5	2.5	35.5

The weight of water comprises 10% of the physical model

According to similarity theory principles, similarity coefficients satisfy the following relationship.

$$\frac{c_\sigma}{c_L \times c_\rho} = 1 \quad (2)$$

Moreover, the prototype and the physical model must satisfy kinematic similarity (Wu et al. 2015), and the advancing speeds of the prototype v_p and the physical model v_m can be written as

$$c_L = \frac{v_m}{v_p} \quad (3)$$

On the basis of Eqs. (1) and (2), the compressive strength of each layer in the physical model could be computed as follows

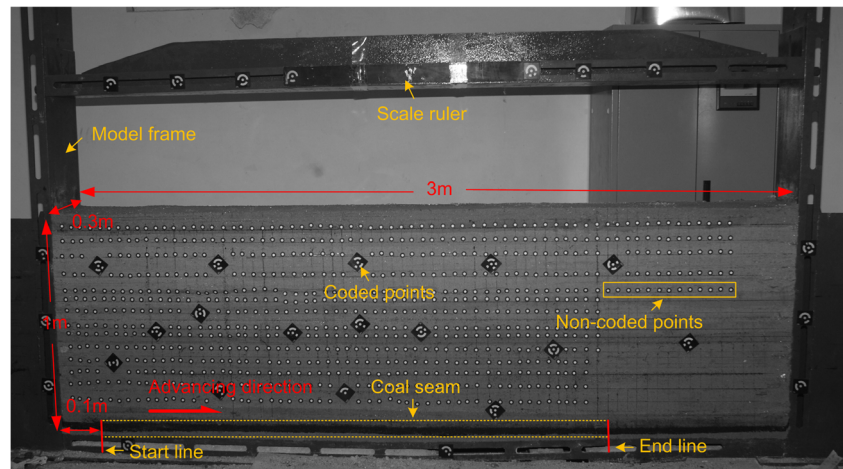
$$\sigma_m = \frac{\sigma_p \times \rho_m}{c_L \times \rho_p} \quad (4)$$

The physical model was 3 m long, 1 m high, and 0.3 m wide, with a geometry similarity coefficient $c_L = 200$, and the coal seam was horizontal (Fig. 2). According to the borehole data provided by the Shendong Coal Company, the composition of the model (dry mixtures) can be calculated as Table 1. The weight ratio of water to other materials is 1:9.

Photogrammetric measurement of strata movement and cracks development

Photogrammetry is one of the cheapest, simplest, and most effective means of measuring strata displacement. Many researchers have used photogrammetry to observe subsidence, displacement, crack propagation, and stability of multiple coal seam minings from physical models (Huang et al. 2013; Thongrapha et al. 2015). The method has also frequently

Fig. 2 Front view of physical model. The non-coded points on the model are taken as observation points to record the deformation of the physical model



been used in stability assessment of caverns and tunnels (Huang et al. 2013; Lee and Bassett 2007; Liu 1986). An industrial photogrammetry system, XJTUDP, was adopted to monitor the ground and strata displacement in this test (Li and Li 2011).

The displacements of strata and the ground at every stage of subsidence were recorded by taking photographs at various angles, after which the coordinates of measuring points were computed using the XJTUDP industrial photogrammetry system with an accuracy of less than 0.086 mm (Li and Li 2011; Wu et al. 2015; Zhang et al. 2010). There were a total of 30 coded points, 785 non-coded points, and a scale ruler on the surface of the model (Fig. 2). Coded points functioned as corresponding image points in different photographs for bundle adjustment. Non-coded points were evenly distributed at 40-mm horizontal intervals to represent corresponding points in the strata, with every row parallel to the upper surface of the model. The scale ruler was used to determine the measurement scale.

All points were unified to the coordinate system shown in Fig. 3 to measure ground movement and fissures in the

vertical profile. The first non-coded point in the first row was the origin, with the x-axis pointing in the advancing direction and the y-axis pointing vertically upward.

The strata collapse and crack developmental status were recorded manually, combined with artificial recognition from photographs. The lengths, widths, and depths of cracks were measured using a small steel ruler, and the measurement time was also recorded.

Experimental procedure and set-up

Once fully mixed, each layer was sequentially paved into the model frame. The start line was only 100 mm from the left-hand side of the model frame, and there were no frames on the model's back and front, equivalent to full subsidence in the tendency direction (Fig. 2). The 3.5 cm thick coal seam was horizontally paved in the model and was excavated by 50 mm every hour. The model deformation was recorded by taking pictures and measuring the locations, lengths, widths, and depths of fissures after each exploitation. Table 2 lists the exact time of every excavation and the homologous advance

Fig. 3 Strata displacement measuring system and unified coordinate system. Green points and numbers denote the location and serial numbers of the coded points, respectively. White points are non-coded points; the yellow line denotes the scale ruler

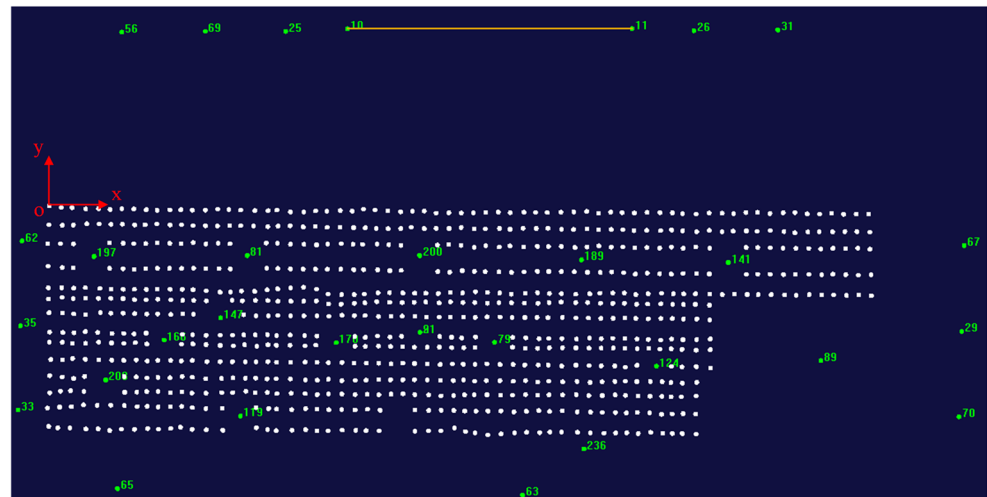


Table 2 Time of each excavation and homologous advance distance

Date	Time	Advanced distance (mm)	Date	Time	Advanced distance (mm)
1st day	19:40	50		17:10	1100
	21:40	150		18:14	1150
	22:50	200		19:30	1200
	23:50	250		20:40	1250
2nd day	0:50	300		21:40	1300
	1:50	350		22:40	1350
	2:50	400		23:40	1400
	3:50	450	3rd day	0:45	1450
4:50	500	1:55		1500	
5:50	550	2:20		1550	
6:50	600	3:50		1600	
7:50	650	4:50		1650	
9:15	700	5:55		1700	
10:12	750	6:50		1750	
11:15	800	7:50		1800	
12:18	850	8:48		1850	
13:13	900	9:54		1900	
14:23	950	10:50		1950	
15:11	1000	12:15		2030	
16:10	1050	13:50	2110		

distance. The whole mining process lasted for 3 days, and two extra groups of photographs were taken before and after coal mining as supplementary information.

For comparison with in-situ mining, all related parameters and dimensions are transformed to the prototype size. This experiment concentrates on strata movement in a vertical profile (Fig. 3); thus, the left side mentioned below refers to the negative direction of the x-axis; the right side denotes the positive direction (Fig. 2).

In situ measurement of ground settlement and cracks

To verify the results obtained from the physical model, we set two perpendicular observation lines above a typical working face in the study region and used second-order leveling¹ to record time-dependent subsidence on the surface. The precision of second-class leveling is within 2 mm. The distribution of the stations are shown in Fig. 4. GPS and steel ruler were used to record the location, width, and length of surface cracks, respectively. Moreover, some fissures were grouted with the mixture of plaster and water and then excavated to measure the depth.

¹ Specifications for the first and second order leveling in China, 2006.

Test results

Strata breakage and collapsing

As the underground coal seam was excavated, the original stress equilibrium of the strata was destroyed as the supporting force in mined-out area decreased, causing strata and ground movement. In this model, breakage fissures first formed on the sides of the coal face as rock layers broke. The upper strata separated as a result of bending differences, and the ground subsided synchronously. The induced fractures displayed an asymmetric distribution, where the break angles close to the start line were 65° and those near the current working face 59°. The angle of draw was 70° (Fig. 5a). When the working face advanced forward, previous bending separation and induced fractures began to close under the pressure of the caved rock above, and new cracks formed above the advancing position. The induced fractures shifted forward with the working face, and the height also increased gradually (Fig. 5b).

Propagation rules for deformation of rock layers

Strata deformation also propagated upward with a diminishing amount of damage. In the model, the rock layers were represented by corresponding measuring positions on their surface. The first, third, sixth, ninth, and 13th rows of non-coded points from the top downward (Fig. 2) were calculated before the occurrence of ground fissures (Fig. 6). The working face has advanced for 200 m at this time. The ninth row of the rock stratum and the strata above that layer only showed bending deformation, whereas the rock layers below had broken and caved.

As shown in Fig. 5, in the fractured and caved strata, the caving width and horizontal influence distance of the upper rock layers were smaller than those of the lower ones. Conversely, the horizontal influence distance of bending strata near the surface increased from the bottom up. Fitting the y-coordinates of each layers and their corresponding maximum subsidence, as well as horizontal influence distance demonstrated that during the process of deformation propagation, the maximum settlement value of rock layers described a quadratic polynomial decline while the horizontal influence distance exhibited a linear rise (Fig. 7). Hence, strata deformation propagates from the bottom up, and the ground experiences the smallest subsidence but the largest horizontal influence range.

Major factors influencing surface crack development

Quantitative calculation of ground deformation

Several major influencing factors were quantified to analyze specifically the primary developmental cause of surface

Fig. 4 Distribution of the observation points. The *red points* denote the observation points, and the *black rectangle* in the middle denotes the working face. The two observation lines are about 1100 m and 900 m long, respectively, and the distance between two neighboring observation points is 20 to 30 m. The eight additional control points marked with a *yellow star*, K1- K8, were set outside the subsidence region. Other labels, such as “530 m”, are the distance between K7 and the observation line in advancing direction

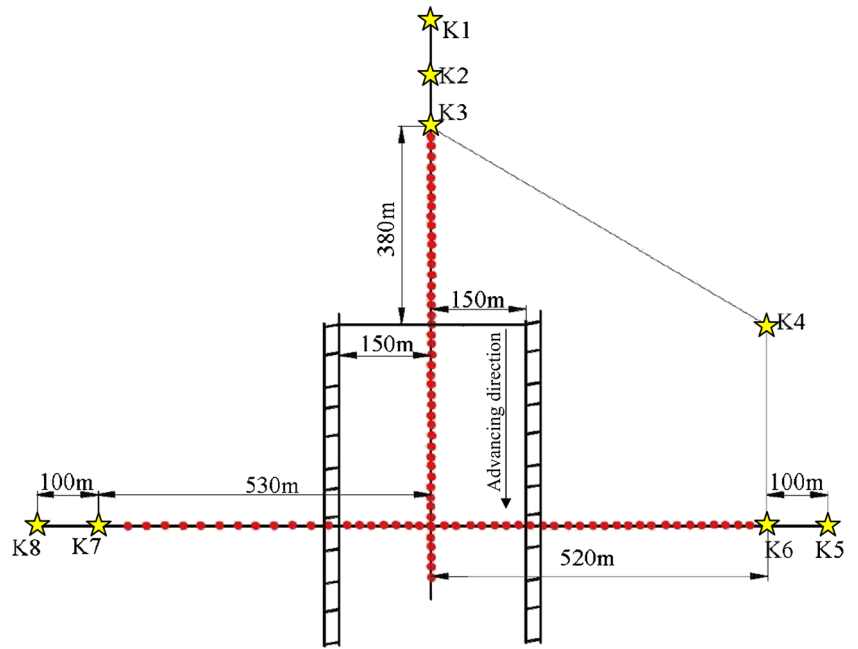
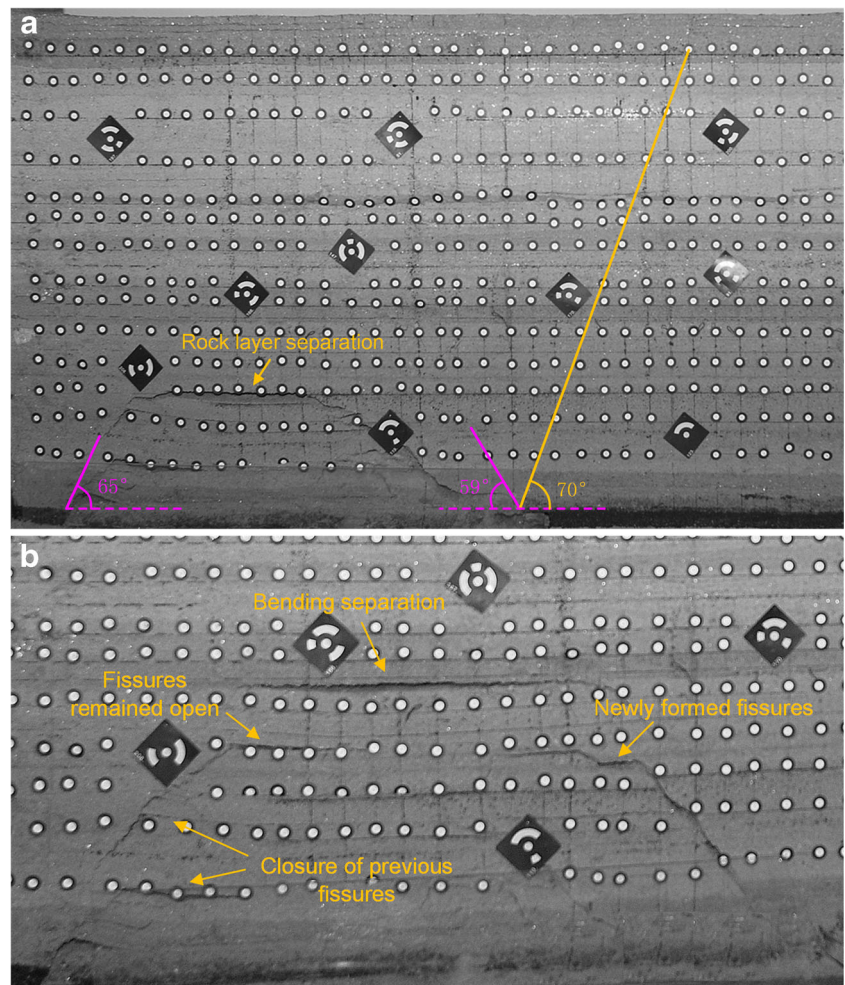


Fig. 5 (a) Break angle of strata, (b) horizontal, and (c) vertical propagation of induced fractures. The white points on the model are used as observation points to record deformation



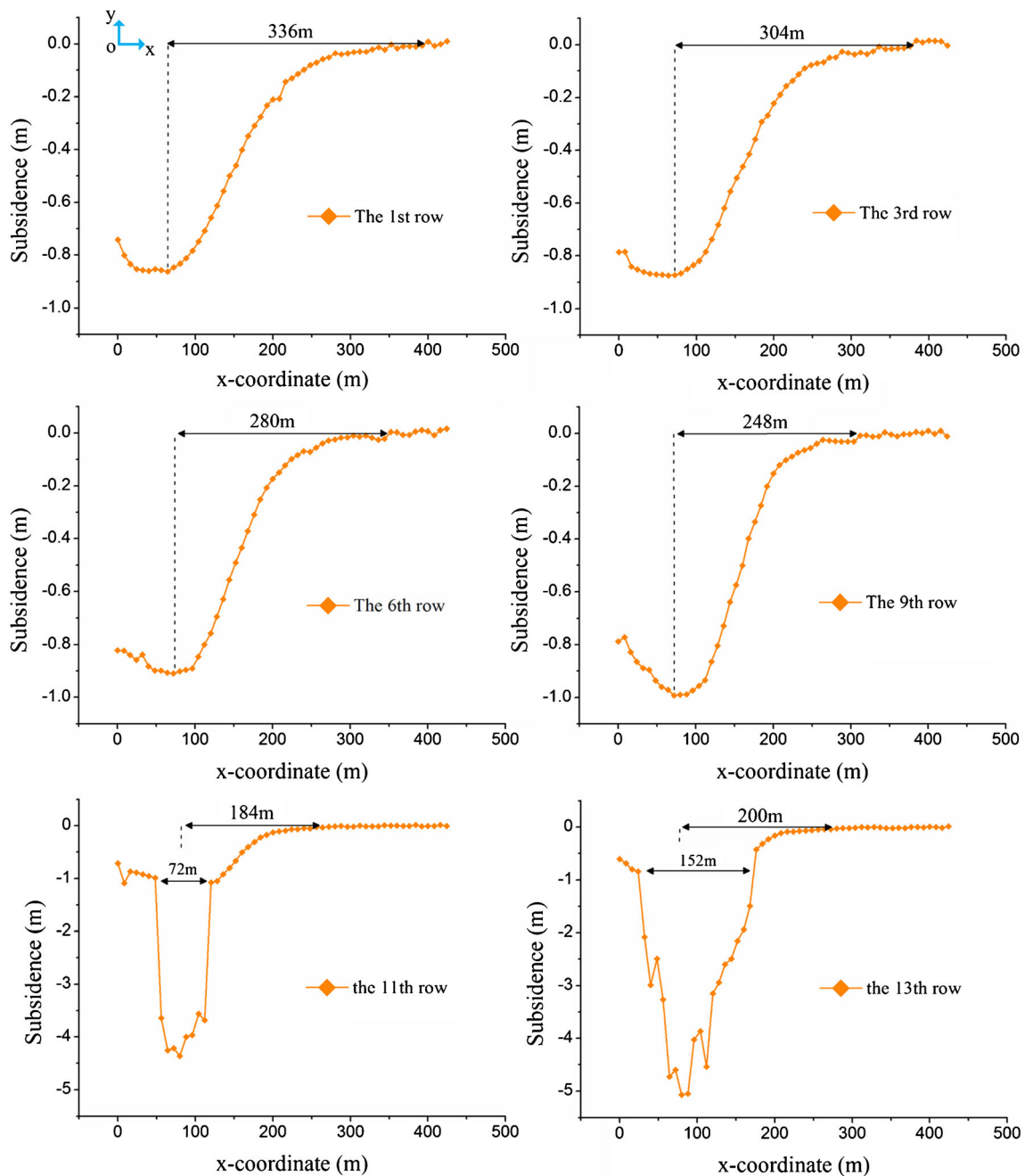


Fig. 6 Deformation propagation of rock strata. The horizontal influence distance is defined as the horizontal length between the point with the maximum subsidence and the nearest point of zero subsidence to the right of that point

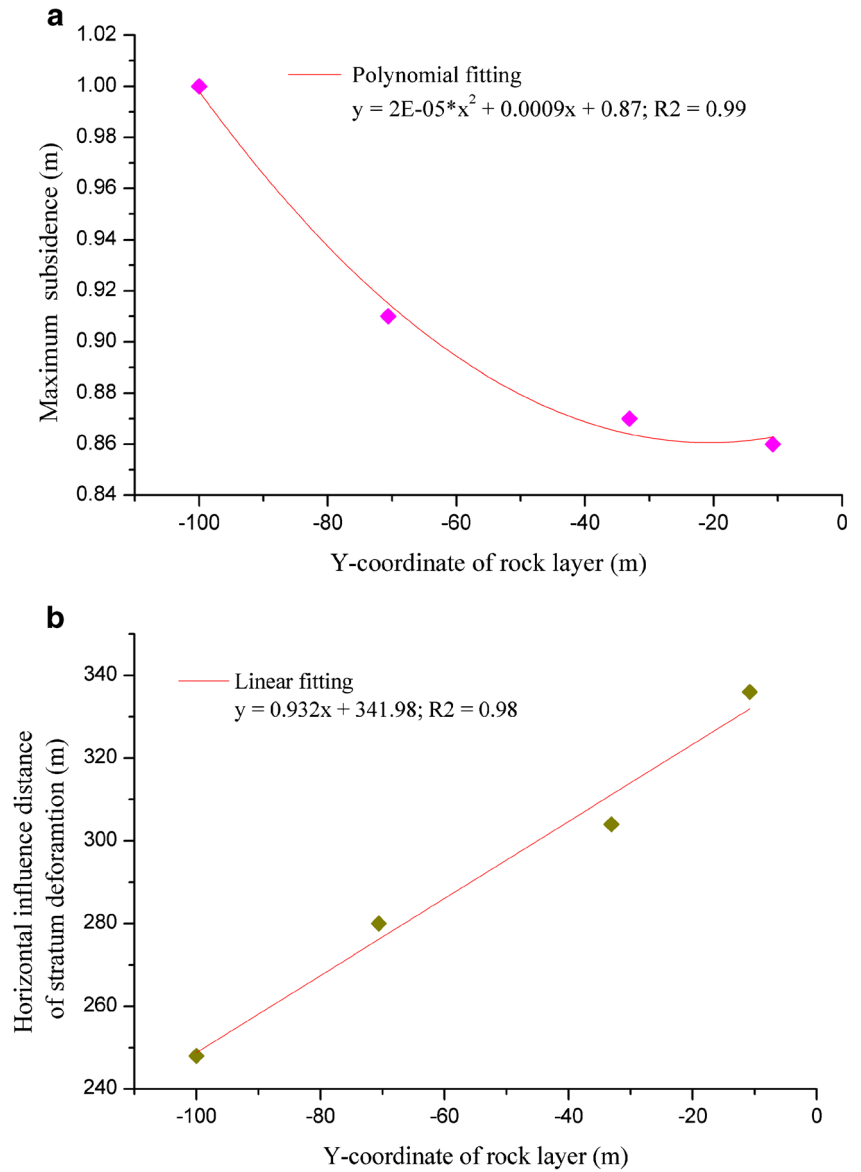
cracks. Of these factors, the ground settlement and height of breakage fissures could be obtained directly by measurement, whereas the ground curvature and horizontal deformation required extra computation. To facilitate accurate measurement and numerical calculation, the first row of non-coded points was regarded as the ground, which was 10.8 m (in prototype size) distant from the upper surface of the model.

Because of the influence of the subsidence trough and subsidence steps, the surface curvature at a fissure could not be obtained directly from three neighboring points. As each

fissure was located near to a corresponding non-coded point with a horizontal distance of less than 0.2 m, their x-coordinates were represented by homologous non-coded points. The ground curvature was calculated from the subsidence value of five continuous points, with the fissure in the middle, two points, m and n , on the left, and two points, p and q , on the right. The curvature of the fissures was calculated as

$$k = \frac{i_{p-q} - i_{m-n}}{l_{p-q} - l_{m-n}} \tag{5}$$

Fig. 7 Propagation rule of strata in terms of (a) subsidence and (b) horizontal influence distance



$$i_{m-n} = \frac{w_n - w_m}{l_{m-n}} \tag{6}$$

$$i_{p-q} = \frac{w_p - w_q}{l_{p-q}} \tag{7}$$

where i_{m-n} and i_{p-q} represent the average slope of points $m-n$ and $p-q$; l_{m-n} and l_{p-q} denote the horizontal distances of points $m-n$ and $p-q$; and w_m, w_n, w_p , and w_q represent the subsidence value of points m, n, p , and q .

The ground horizontal deformation between the two points was calculated as

$$\varepsilon = \frac{l_i - l}{l} \tag{8}$$

where ε stands for horizontal deformation; l is the original distance between the two points before coal excavation;

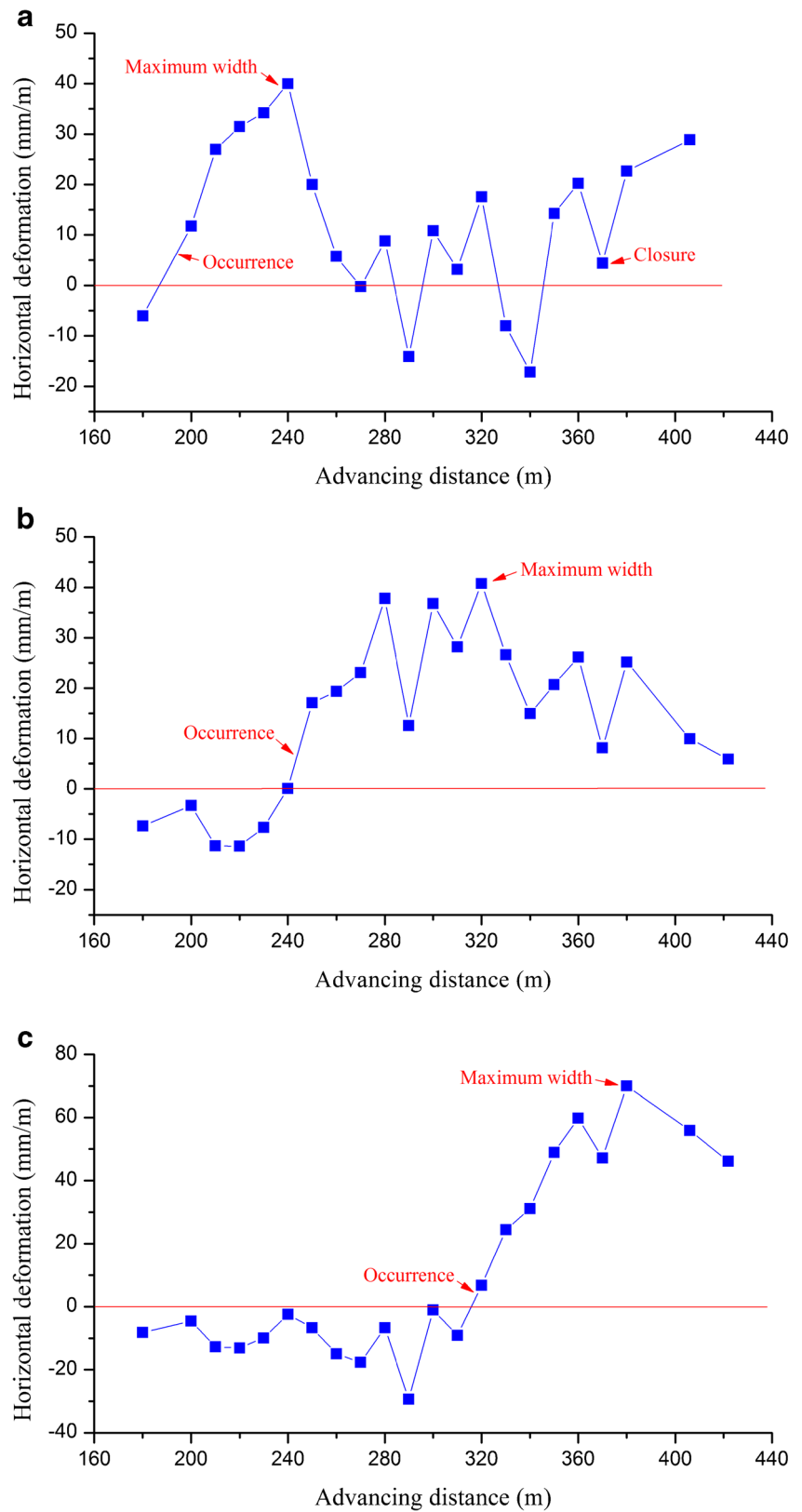
and l_i denotes the horizontal distance between the two points at time i . The ground suffers tension for $\varepsilon > 0$ and experiences compression for $\varepsilon < 0$. The horizontal distortion of the ground during the developmental process of three fissures is depicted in Fig. 8.

The relationship between strata movement and ground cracks

The developmental cycle of OCF involved two phases, expansion and closing. Fissure 1 was selected as an example to analyze the developmental process of ground OCF through the whole fissure cycle.

Fissure 1 occurred at the right-hand edge of the settlement basin, 39 m ahead of the excavation position. In a development cycle, the ground curvature and horizontal deformation demonstrated a similar trend with the change of width of

Fig. 8 Horizontal distortion of ground close to (a) fissure 1, (b) fissure 2, and (c) fissure 3. Fissures 1, 2, and 3 are 206.2 m, 277.8 m, and 373.2 m distant from start line, respectively



ground cracks, and the ground subsidence increased constantly (Table 3). However, the maximum height of breakage cracks presented a completely reverse trend (Fig. 9). In the

expansion phase, the maximum height of the breakage cracks decreased conversely, and in the closing stage, it started to rise.

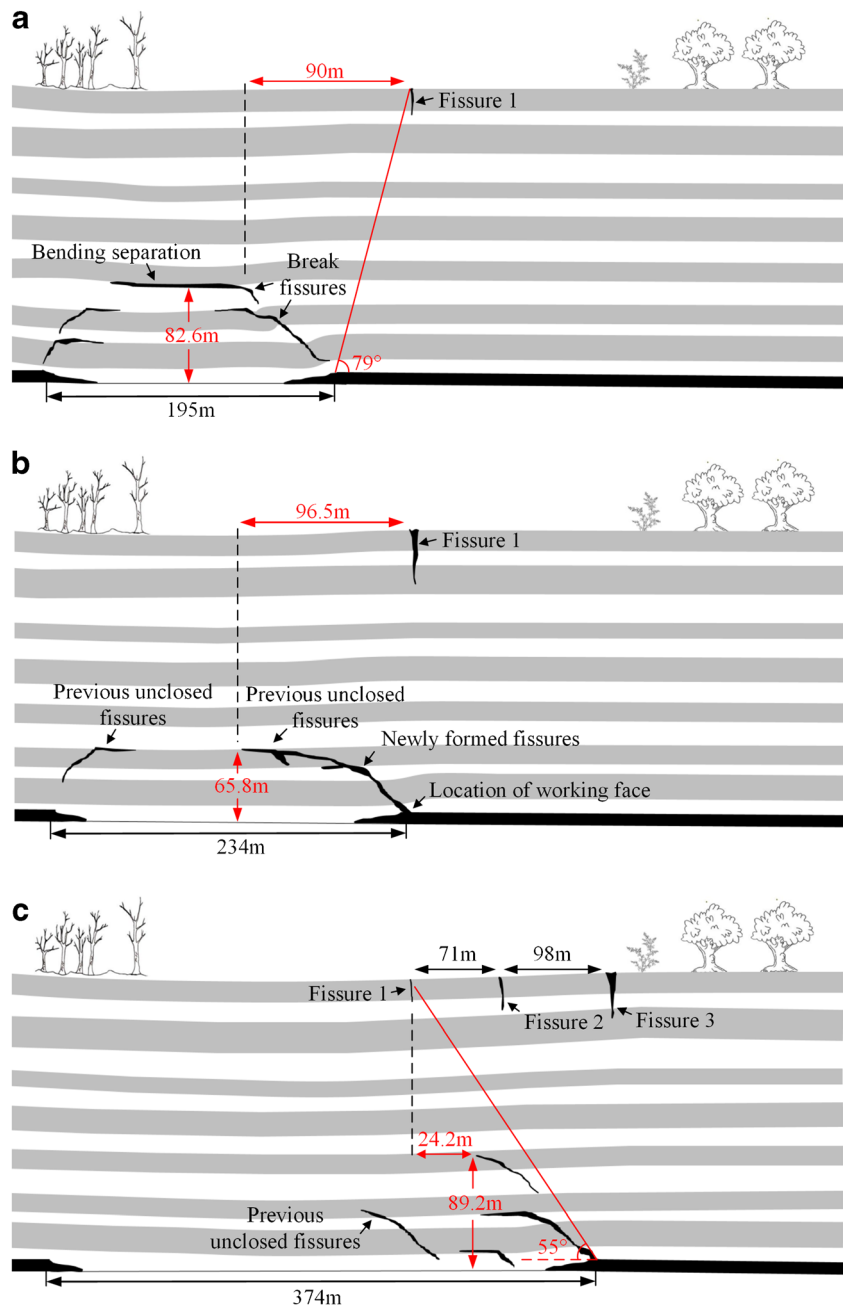
Table 3 variation of influence factors in a fissure development cycle

Name	Ground subsidence (mm)	Horizontal deformation (mm)	Ground Curvature ($\times 10^{-3}/\text{m}$)
Occurring	109	6.16	0.65
Maximum width	176	39.96	1.62
Closure	3002	4.41	-3.07

Moreover, from the field data, the maximum width of ground fissures were between 13.2 to 58.5 mm, and the

depth ranged from 68.4 to 1120.8 mm (Hu et al. 2014). Therefore, it can be concluded that the occurrence of ground fissures cause tension release of the ground and pose more stress to the lower strata, causing breakage fissures to close and have small height. The height of breakage cracks rose again as the exploration position was ahead of fissure 1. The same phenomenon was observed during the development of fissures 2 and 3. Hence, strata failure is the cause of ground fissures, and, in turn, the fissure can contribute to fracturing and caving of lower rock layers to form a new stable structure, that is, a settlement basin.

Fig. 9 Breakage fissures distribution at moments of (a) occurrence, (b) maximum width, and (c) closure of fissure 1. The observations are obtained from the physical model, but dimensions given are translated to the in situ situation



Developmental cycle of surface cracks

Between formation and closure of fissure 1, the working face advanced by 180 m (Fig. 10a). Because of the fast mining speed of 12 m/day, the fissure had a short developmental cycle of around 11 days. The expansion duration of fissure 1 was 2.30 days, similar to the values of fissures 2 and 3, 2.35 and 2.94 days, respectively. The closing stage lasted for 8.30 days, approximately 3.6 times the expansion phase. This is well in line with the field observation. We selected five ground cracks at Bulianta mine to record the change of their width in detail, and the results demonstrated that these ground cracks took approximately 3 days to expand and 12 days to close (Hu et al. 2014). The development cycle is highly asymmetric.

However, to coal mines with lower mining speed, the development process of ground cracks is obviously different. We choose a typical mine in eastern China, Baodian mine as example. Baodian mines have similar geological conditions with Bulianta mines, but the mining speed is about 2 m/day (Ni and Wang 2014). As shown in Fig. 10b, the in situ observation of ground cracks above Baodian mines demonstrates that the

opening stage and closing stage of cracks take a similar amount of time.

Formation and closure of ground fissures

The major factors influencing fissure development can be determined by comparing the developmental conditions of three surface cracks. First, the height of breakage fissures was examined. As illustrated in Table 3, the breakage cracks had increasing height as the three fissures formed, thus it did not have a primary impact on fissure formation. Additionally, the distance between the three fissures and corresponding nearest breakage cracks showed an increasing trend: this may have been induced by fast mining speed. The lower rock layers did not cave fully, so the upper layers suffered only slight bending deformation rather than fracturing.

Second, the values of ground subsidence and curvature all showed large differences when the three fissures first occurred. Only the horizontal deformation was much the same for all the fissures (Table 4). The three fissures all appeared

Fig. 10 The comparison of developmental cycle of ground cracks under different excavation speed. (a) The observations are obtained from the physical model, but dimensions given are translated to the in situ situation. (b) This figure is reshaped from the in situ observation of (Ni and Wang 2014) in Baodian mines. The black segments denote the position and width of all ground cracks when the working face has advanced to the about 100 m position

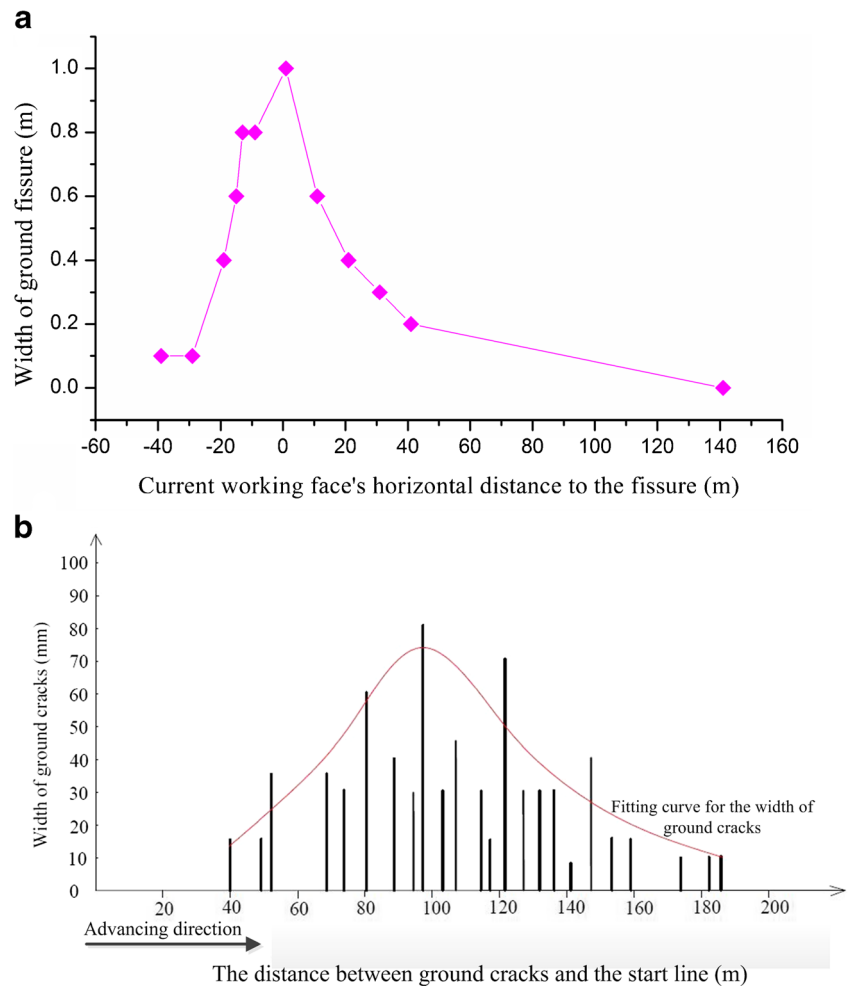


Table 4 Influence factor comparison

Name	The height of break cracks (m)	Horizontal distance of fissure and break crack (m)	Ground subsidence (mm)	Horizontal deformation (mm)	Ground Curvature ($\ast 10^{-3}/m$)
Fissure 1	82.6	90	109	6.16	0.65
Fissure 2	109.2	153.8	85	6.26	0.60
Fissure 3	140.2	170	11	6.33	0.09

when the horizontal distortion altered from negative to positive and reached a value of approximately 6.25 mm/m.

From the above analysis, it can be concluded that the formation of ground fissures can only be assessed using the level of horizontal tensile deformation, rather than the height of breakage fissures, ground subsidence, or curvature. In addition, the horizontal tensile deformation can be used as an index of crack width. When the width of the three fissures also peaked, the corresponding ground distortion was also showed maximum values of 39.96, 40.75, and 69.96 mm/m, respectively, which were similar to the field measurement results, 45.91 mm/m (Shi et al. 2008).

In this way, the closure condition of surface cracks can also be determined. During the closing phase of fissure 1, ground subsidence and the height of breakage fissures still continued to increase (Fig. 10), and the horizontal deformation fluctuated irregularly (Fig. 9a). Only the ground curvature decreased

Fig. 11 (a) Surface settlement obtained from the physical model. The negative horizontal coordinate denotes that measurement points was located on the left side of start line, and the thickness of the mined coal seam is 7 m (translated to the in situ situation). (b) Ground subsidence obtained with in situ measurement. The excavation thickness of the coal seam is 5 m

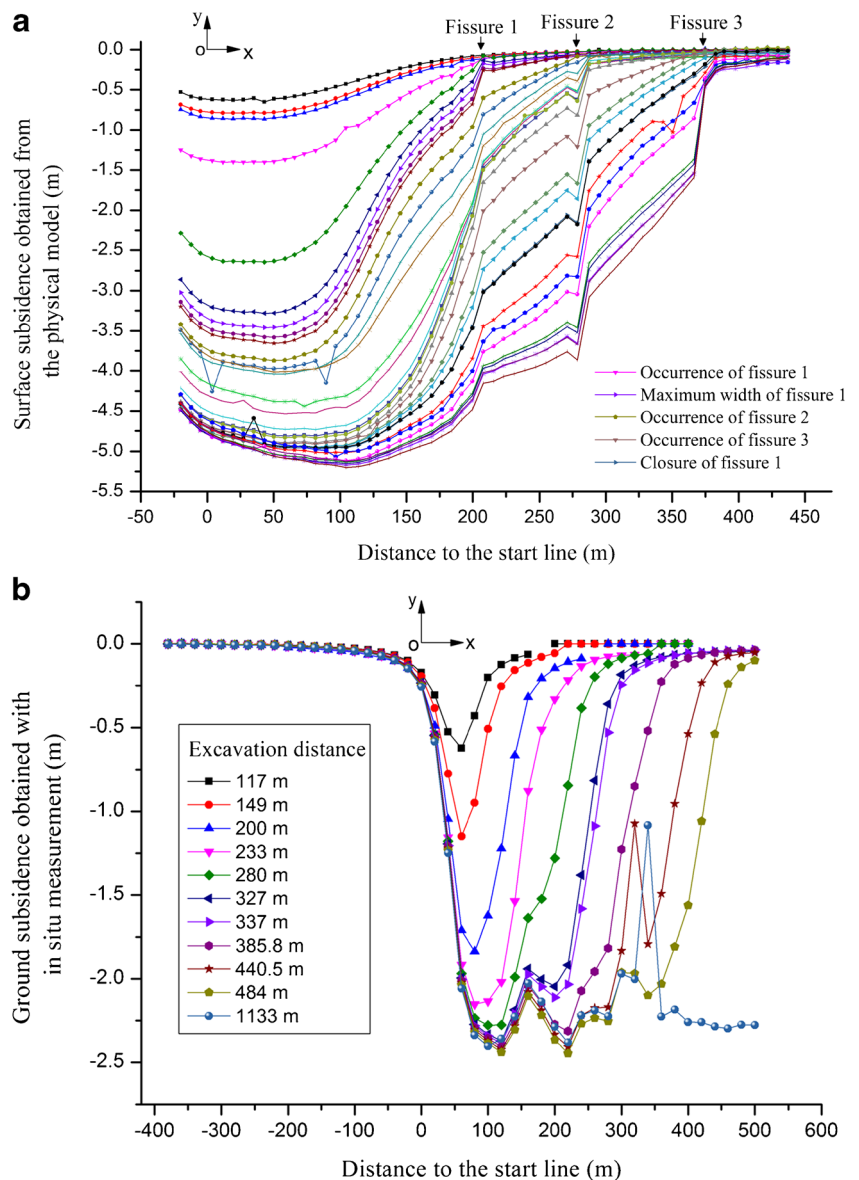
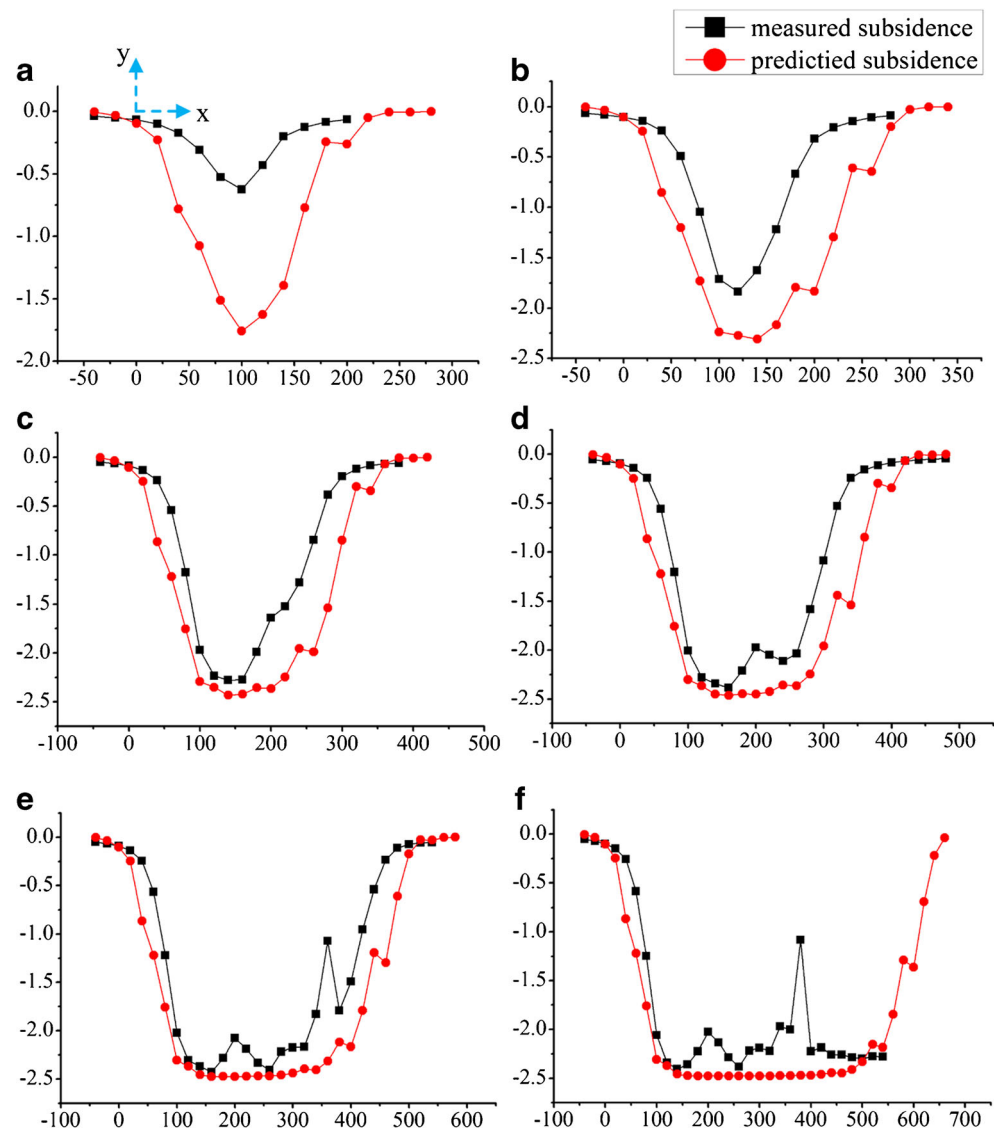


Fig. 12 The comparison of prediction subsidence and in situ measurement value. The X-axis represents the distance to the start line, and the Y-axis represents subsidence value. a - f denote the measured and predicted subsidence of ground points when the working face has advanced for 117 m, 200 m, 280 m, 227 m, 440.5 m, and 1131 m, respectively



gradually to a negative value, showing a marked correlation with fissure closure. Therefore, ground curvature was the major influencing factor in closure of ground fissures. This is because as the working face moved forward, the ground reached full subsidence and formed a settlement basin, causing the ground curvature near the fissures to diminish and become negative. This can also be verified by the development of fissure 2 in the closing period.

Surface settlement

The subsidence curve of the physical model during the course of ground-fissure development is illustrated in Fig. 11a. As the left coal pillar was only 20 m long, the subsidence basin deviated to the left.

From Fig. 11a, under fast mining, the working face had advanced for 442 m when the ground reached its maximum

subsidence. This value is nearly 2.2 times the mining depth, far greater than of the value for ordinary mechanized coal mining, $1.2\text{--}1.4H$ (H stands for mining depth), and this is verified by our in situ measurement (Fig. 11b). The field measurements shows that the ground did not reach full subsidence until the coal seam has been excavated for $2.4H$, 484 m.

Moreover, we compared the field measurement subsidence with the dynamic prediction method proposed in (Li et al. 2014), which is accurate for settlement prediction caused by low-intensity mining. The corresponding prediction parameters are given in (Wang 2014). As shown in Fig. 12, there are large errors between the measured and predicted subsidence at first, but the difference narrows with the working face going forward, and it is worth noting that in Fig. 12 b-e, the errors on the right side are obviously larger than that on the left.

The above-observed phenomenon is because the overburden strata did not break fully and formed a temporarily stable

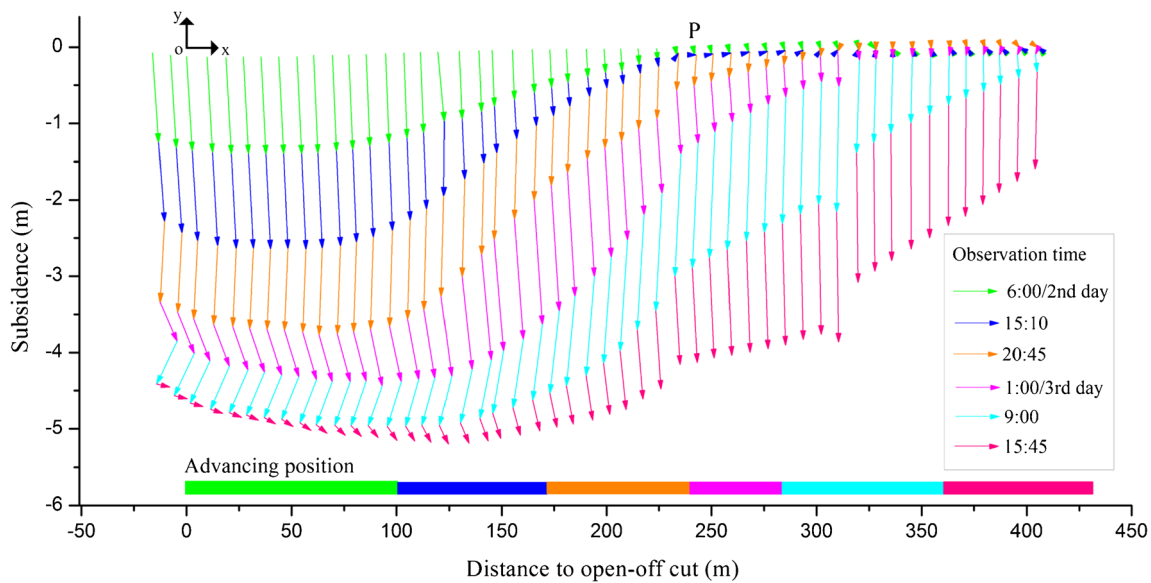


Fig. 13 Displacement vector of ground points. The *rectangular stripes* at the bottom of the figure denote that when continuing to excavate such a distance, the displacement vectors in corresponding color take place on

the ground. The observations are obtained from the physical model, but dimensions given are translated to the in situ situation

structure in a short time, as it takes only 24 days to advance a distance of $1.4H$ with mining speed of 12/days. However, as time goes on, the overlaying strata would finally fractured completely and cause ground to reach maximum subsidence, and at this time, the working face may have advanced to $2.2H$ position or more.

This special phenomenon of strata movement caused by fast excavation may cause large error for dynamic prediction results, but the major factor lies with the time. In this experiment, its influence on the prediction results of maximum subsidence will decrease to zero after 1 month. It can be seen that the actual settlement accords well with the predicted values in Fig. 12 f, where the working face has advanced for 3 months. However, such prediction errors would not happen to cases where the mining speed is less than 5 m/day, because the

working face has advanced for more than one month before the ground start to subside.

Developmental mechanism of ground fissures

Movement of ground points

As shown in Fig. 13, taking point P as an example, the displacement of ground points went through five periods successively as the working face moved forward: horizontally rightward, left-downward, right-downward, left-downward, and right-downward. When the working face was near to point P, the ground suffered a horizontal tension: surface fissures also occurred during this period.

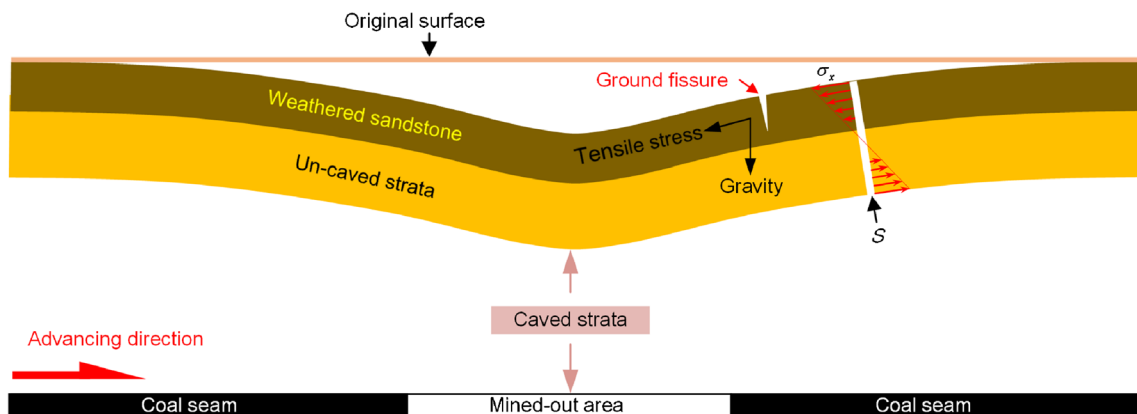


Fig. 14 Mechanical analysis of ground fissures formation and development. The strata suffers tension as σ_x pointed leftwards and bears compression as it points rightwards

Mechanical mechanism

Before occurrence of ground fissures, under the influence of gravity, the overlying strata near the mined-out area caved directly, whereas the upper strata bent instead of caving and suffered from tension. The stress σ_x in a section S increased linearly from inside the strata to the ground surface, and the ground experienced the maximum tensile strength (Fig. 14). Under self-gravity and tensile stress, the ground would be destroyed first, and ground fissures generally developed as V-shaped and extended to the coal pillar zone. These features were also observed at the surface at the Bulianta mine (Fan et al. 2015; Wang et al. 2010; Wang 2014).

After the formation of fissures, the ground on both sides of the fissures showed discontinuous movement as a result of loss of original cohesion. When the working face fell behind the fissures, the ground to the left of the fissure was affected by self-gravity and tension inside soil, whereas the ground to the right suffered only from self-gravity and the supporting force of lower strata (Fig. 14). The ground to the left suffered greater tension, thus the width of cracks increased constantly. After the working face moved ahead of the fissures, the tensile load transferred to the right-hand ground, thus the fissures started to close.

Conclusions

Under mining conditions with thick coal seams, shallow cover, and rapid exploitation, the ground deformation and strata failure follow special rules. Physical model and high-precision photogrammetry, as well as field measurement were employed to explore the development of surface fissures and regularity of strata movement.

Mining-induced strata deformation propagates from the bottom up: in the deformed rock layers, the maximum settlement value shows a quadratic polynomial decrease, whereas the horizontal influence distance displays a linear increase. Under the influence of rapid exploitation, rock layers cannot break fully in a short time and the ground does not achieve full subsidence until the working face has advanced to 2.2 times the mining depth, which is far greater than the empirical parameter of 1.2–1.4. OCF are self-closing with a complete developmental cycle consisting of short period of expansion and a long period of closing, the latter being 3.6 times longer than the former. Fast mining can shorten the developmental cycle of ground cracks, as it is inversely proportional to the mining speed. The major cause of ground fissures is horizontal deformation, rather than the height of breakage cracks, ground subsidence, or ground curvature. In contrast, the closure of surface cracks is principally controlled by the ground curvature.

As the horizontal deformation is one of the most stable factor reflecting the potential occurrence of ground fissures,

thus it can be used to predict ground fissures. The position, maximum width, and developmental cycle of surface cracks can be accurately predicted if combined with finite element modeling and the probability integral method. Moreover, as the overburden strata cannot collapse in a short time, the predicted ground subsidence with probability integrality method in the initial phase may be far larger than the actual settlement.

Comparison with in situ measurement data demonstrates that similar material can be used for effective modeling of strata movement and ground fissures induced by underground coal excavation to obtain qualitative results. The results of the present study can provide a theoretical foundation for prediction of ground cracks and strata movement due to fast coal excavation.

Acknowledgements This work was supported by the Natural Science Foundation of China and Shenhua Group Co., Ltd. (Grant number U1361203). The authors would like to thank the editor and reviewers for their contributions on the paper.

References

- Cui X, Miao X, Zhao Y, Jin R (1999) Discussion on the time function of time dependent surface movement. *J China Coal Soc* 5:453–456
- Dai H, Lian X, Liu J, Liu Y, Zhou Y, Deng W, Cai Y (2010) Model study of deformation induced by fully mechanized caving below a thick loess layer. *Int J Rock Mech Min* 47:1027–1033
- Deng K, Tan Z, Jiang Y, Dai H, Shi Y, Xu L (2014) Deformation monitoring and subsidence engineering. China University of Mining and Technology Press, Xuzhou
- Fan L, Zhang X, Xiang M, Zhang H, Shen T, Lin P (2015) Characteristics of ground fissure development in high intensity mining area of shallow seam in Yushenfu coal field. *J China Coal Soc*:1442–1447
- Ghabraie B, Ren G, Zhang X, Smith J (2015) Physical modelling of subsidence from sequential extraction of partially overlapping longwall panels and study of substrata movement characteristics. *Int J Coal Geol* 140:71–83
- He G, Yang L, Ling G, Jia C, Hong D (1991) Mining subsidence theory. China University of Mining and Technology Press, Xuzhou
- Hu Z, Wang X, He A (2014) Distribution characteristic and development rules of ground fissures due to coal mining in windy and sandy region. *J China Coal Soc*:11–18
- Huang F, Zhu H, Xu Q, Cai Y, Zhuang X (2013) The effect of weak interlayer on the failure pattern of rock mass around tunnel - scaled model tests and numerical analysis. *Tunn Undergr Sp Tech* 35:207–218
- Lee Y, Bassett RH (2007) Influence zones for 2D pile-soil-tunnelling interaction based on model test and numerical analysis. *Tunn Undergr Sp Tech* 22:325–342
- Li G, Li Z (2011) The principles and applications of industrial measuring systems. Surveying and Mapping Press, Beijing
- Li L, Wu K, Zhou D (2014) AutoCAD-based prediction of 3D dynamic ground movement for underground coal mining. *Int J Rock Mech Min Sci*:194–203
- Liu P (1986) Model test study on double lining of tunnels. *Tunn Undergr Sp Tech* 1:53–58
- Liu Y, Zhou F, Liu L, Liu C, Hu S (2011) An experimental and numerical investigation on the deformation of overlying coal seams above double-seam extraction for controlling coal mine methane emissions. *Int J Coal Geol* 87:139–149

- Ni X, Wang F (2014) Technical study and practice of thick coal mining under watercourse in Yanzhou mining area. China University of Mining and Technology Press, Xuzhou
- Shi X, Xu J, Zhu W (2008) Site measurement on surface subsidence occurred by coal mining with high cutting height under complicated conditions in Bulianta Mine. *Coal Sci Technol*:80–83
- Thongprapha T, Fuenkajorn K, Daemen JJK (2015) Study of surface subsidence above an underground opening using a trap door apparatus. *Tunn Undergr Sp Tech* 46:94–103
- Wang X (2014) Monitoring, evolution and self-healing characteristic of land damage due to high tension coal mining in windy and sandy area. China University of Mining and Technology, Beijing, p 136
- Wang L, Chu Y, Zhao N (2010) Numerical simulation study on ground fissures induced by mining. *J Shenyang Jianzhu Univ (Nat Sci)*: 1138–1141.
- Whittaker BN, Reddish DJ (1989) *Subsidence Occurrence. Elsevier, Prediction and Control*
- Whittaker BN, Reddish DJ, Fitzpatrick DJ (1985) Ground fractures due to longwall mining subsidence. In: *International Mine Water Association: Granada, Spain*. pp 1057–1072.
- Wu K, Hu Z, Chang J, Ge J (1997) Distribution law of ground crack induced by coal mining. *J China Univ Min Technol*:56–59.
- Wu K, Cheng G, Zhou D (2015) Experimental research on dynamic movement in strata overlying coal mines using similar material modeling. *Arab J Geosci* 8:6521–6534
- Zhang D, Liang J, Guo C, Liu J, Zhang X, Chen Z (2010) Exploitation of photogrammetry measurement system. *Opt Eng* 49